

Macroscopic quantum tunnelling of protons in the KHCO_3 crystal

François Fillaux^{a,*}, Alain Cousson^b, Matthias J. Gutmann^c

^a LADIR-CNRS, UMR 7075 Université P. et M. Curie, 2 rue Henry Dunant, 94320 Thiais, France

^b Laboratoire Léon Brillouin (CEA-CNRS), C.E. Saclay, 91191 Gif-sur-Yvette Cedex, France

^c ISIS Facility, Rutherford Appleton Laboratory, Chilton, Didcot OX11 0QX, UK

Received 2 September 2005; received in revised form 3 November 2005; accepted 14 November 2005

Available online 24 January 2006

Abstract

Macroscopic quantum entanglement reveals an unforeseen mechanism for proton transfer across hydrogen bonds in the solid state. We utilize neutron scattering techniques to study proton dynamics in the crystal of potassiumhydrogencarbonate (KHCO_3) composed of small planar centrosymmetric dimer entities (HCO_3^-)₂ linked by moderately strong hydrogen bonds. All protons are indistinguishable, they behave as fermions, and they are degenerate. The sublattice of protons is a superposition of macroscopic single-particle states. At elevated temperature, protons are progressively transferred to secondary sites at ≈ 0.6 Å from the main position, via tunnelling along hydrogen bonds. The macroscopic quantum entanglement, still observed at 300 K, reveals that proton transfer is a coherent process throughout the crystal arising from a superposition of macroscopic tunnelling states.

© 2006 Elsevier B.V. All rights reserved.

Keywords: Quantum entanglement; Neutron diffraction; Hydrogen bonding; Proton tunnelling

1. Introduction

The potassiumhydrogencarbonate (KHCO_3) crystal is a nonferroelectric (nonmagnetic) prototype for proton transfer across hydrogen bonds in centrosymmetric dimers. This is commonly represented as a thermally activated interconversion between tautomers. NMR [1,2], quasi-elastic neutron scattering [3] and spectroscopy studies [4,5], converge to the conclusion that proton transfer occurs via tunnelling across a quasi-symmetric double minimum potential. Two stochastic mechanisms have been proposed: the pairwise synchronous transfer and the uncorrelated two-stepwise single proton transfer. In this paper, we propose a coherent two-stepwise process through macroscopic tunnelling.

Previous studies of the KHCO_3 crystal have revealed long-life macroscopic quantum coherence for entangled pairs of protons [6–8]. Neutron diffraction shows, in addition to Bragg peaks, rods of diffuse scattering due to macroscopic states. Decoherence is cancelled by perfect dynamical separation of protons from rest of the lattice. So far, experiments were carried out at 14 K, a temperature at which protons are ordered.

Proton transfer is observed above ≈ 150 K. We report evidence that quantum coherence survives at room temperature [9]. This is of dramatic consequences with respect to our view of protons in this system and, most likely, in many others.

The organization of this paper is as follows. In Section 2, the crystal structure determined at 300 K evidences thermally activated proton transfer across hydrogen bonds. Simultaneously, the rods of intensity are largely temperature-independent. The theoretical framework for quantum entanglement is presented in Section 3. We define macroscopic single-particle states for pseudoprotons and calculate the differential cross section for comparison with experiments. In Section 4, we introduce the quantum superposition of macroscopic tunnelling states and we emphasize the role of decoherence in the transfer dynamics.

2. Neutron diffraction experiments

2.1. Crystal structure

Measurements of an approximately cubic single crystal ($3 \times 3 \times 3$ mm³) were conducted with the Stoe four-circle diffractometer 5C2 at the Orphée reactor (Laboratoire Léon-Brillouin) [10]. The temperature was controlled to ± 1 K.

The structure at 300 K is similar to those previously reported [8,11,12]. The nonferroelectric crystal is monoclinic, space group $P2_1/a$ (C_{2h}^5), with four KHCO_3 entities per unit

* Corresponding author. Tel.: +33 1 49 78 1283; fax: +33 1 49 78 1118.
E-mail address: fillaux@glvt-cnrs.fr (F. Fillaux).

cell. The planar centrosymmetric dimer entities $(\text{HCO}_3)_2^-$ lie practically in the $(30\bar{1})$ planes and hydrogen bonds are also virtually parallel to the same direction (Fig. 1). The increase of the unit cell dimensions with temperature is marginal.

At 30 K all protons are crystallographically equivalent and indistinguishable. They are localized at a single site (configuration I, see arrows in Fig. 1) and there is no evidence for disordering. At 300 K, the probability density is distributed in a ratio of 0.18:0.82 among two crystallographically distinct sites located at $\approx \pm 0.3 \text{ \AA}$ off-centre of the hydrogen bond. The secondary sites (configuration II) are also crystallographically equivalent and indistinguishable. I and II are related through translation $(a/2, b/2, 0)$. Remarkably, there is no change in peak positions and no evidence for additional peaks. Only intensities are affected. Consequently, proton transfer does not alter the crystal lattice and the geometry of the CO_3^{2-} entities. Configurations I and II are distinct in direct space and isomorphous in reciprocal space.

The sum of probability densities at the proton sites is unity at 300 K. This is at odds with a random distribution of local tautomers [1–3] that should destroy long range correlations at elevated temperatures. If it were the case, a significant amount of the coherent scattering should collapse into off-Bragg peaks diffuse scattering [13] and a decrease of the total density should be observed. Contrariwise, neutron diffraction suggests that proton transfer does not destroy the spatial coherence and the crystal could be a mixture of the isomorphous configurations.

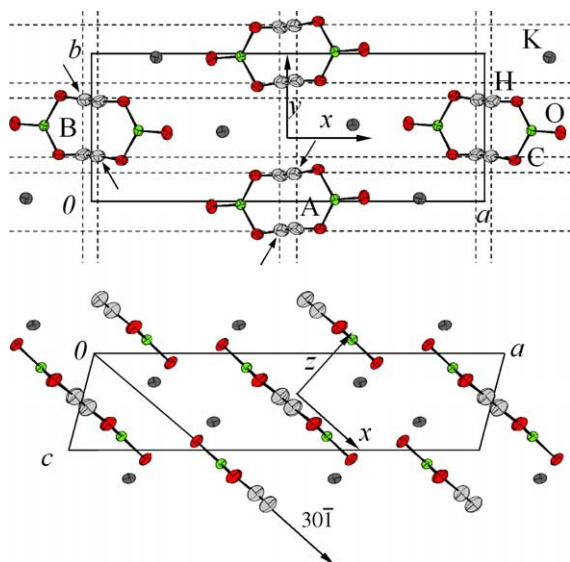


Fig. 1. Schematic view of the crystalline structure of KHCO_3 at 300 K. The thin solid lines represent the unit cell. Apart from proton positions and thermal ellipsoids, the structure is identical to that at 14 K [8]. The arrows point to the sites exclusively occupied by protons at low temperature. Top: projection onto the plane normal to c . The dotted lines joining protons are guides for the eyes to emphasize the superstructure due to quantum coherence of the proton sublattice (see text). Bottom: projection onto the plane normal to b (for the interpretation of the reference to the colour in this legend, the reader is referred to the web version of this article).

2.2. Quantum coherence

The maps of intensity for cuts perpendicular to (b^*) corresponding to (a^*, c^*) reciprocal planes presented in Fig. 2, were measured with the SXD instrument at the ISIS pulsed neutron source [14].

The diffraction pattern at 30 K (Fig. 2A) is practically identical to that previously measured at 15 K [8]. In addition to Bragg's peaks, there is an anisotropic continuum of intensity, centered at $\mathbf{Q}=0$ [15], due to incoherent scattering, and well separated ridges of diffuse scattering. Measurements carried out with a bigger crystal confirmed that there is no significant multiple scattering events.

Streaks of diffuse scattering are commonly observed for disordered systems. However, for hydrogenous materials observation with neutrons is difficult because of the large incoherent scattering [13]. Such streaks are enhanced for deuterated samples, thanks to the more favourable ratio for coherent and incoherent cross sections. Clearly, the ridges in question for KHCO_3 are different in nature: they are observed at low temperature, although there is no disordering, and they are no longer observed for KDCO_3 , in spite of the increase of the coherent cross-section. Moreover, they are little sensitive to proton transfer. In fact, they have all the characteristics anticipated for coherent scattering by the sublattice of protons undergoing quantum correlation [8]: (i) they are clearly separated from Bragg peaks; (ii) orientations correspond to momentum transfer Q_z perpendicular to dimer planes; (iii) positions at $Q_x = \pm(10.25 \pm 0.25) \text{ \AA}^{-1}$ are in accordance with the spacing of double-lines of protons (see below); (iv) the width along (b^*) is similar to that of Bragg peaks. (The ridges have rod-like shapes.)

At 300 K, Bragg peaks and incoherent scattering are largely depressed at large $|\mathbf{Q}|$ -values, a normal consequence of the increase of temperature. In contrast, the ridges of intensity are better visible, and there are clearly three of them. With hindsight, the ridge going through the centre already exists at low temperature, but barely visible. The broadening along Q_x suggests a decrease of the coherence length of the sublattice of protons.

To summarize this section, the salient experimental conclusions (EC) are featured as follows:

- EC1 proton sites for each of the distinct configurations I or II are indistinguishable;
- EC2 interconversion does not alter the spatial coherence;
- EC3 in the absence of disordering, ridges of intensity reveal quantum correlations.

3. Quantum entanglement in a lattice of hydrogen bonded centrosymmetric dimers

Different theoretical frameworks have been proposed for the rods of intensity observed at low temperature [6–8,16–19]. All of them are based on the fact that protons behave as fermions and, therefore, undergo quantum entanglement.

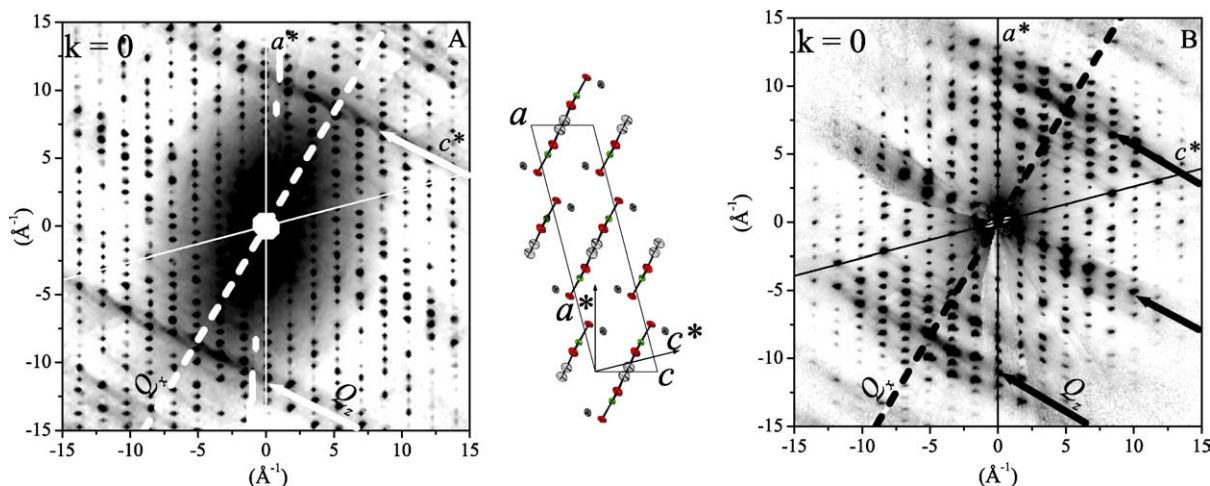


Fig. 2. Diffraction patterns of KHCO_3 at 30 K (A) and 300 K (B) in the (a^*, c^*) plane. The arrows point to the ridges of intensity at 0 and $\approx \pm 10 \text{ \AA}^{-1}$ from the origin. They lie along a direction parallel to z , and as such are perpendicular to the plane of dimers (dashed lines), which contain the x and y directions defined in Fig. 1. The insert visualizes the correspondence between the direct and reciprocal lattices (for the interpretation of the reference to the colour in this legend, the reader is referred to the web version of this article).

However, quantum correlations, either for isolated pairs [16,19], or for collective dynamics of pairs thought of as composed bosons [8] are not in accordance with the persistence of rods of diffuse scattering at room temperature, for the intensity should be depressed by the Debye–Waller factor. These theories must be amended and, for this purpose, we start with the following premises [9]:

- (i) For each configuration of the sublattice, proton sites are indistinguishable.
- (ii) Dynamics are amenable to normal coordinates.
- (iii) Protons are fermions.
- (iv) For each configuration, protons are degenerate. The overlap of the vibrational wave functions is rigorously negligible and so is the exchange energy [17]. Spin–spin interaction is also negligible.

These premises are firmly based on experiments. (i) Is established by diffraction (EC1). (ii) Is a relevant approximation for vibrational dynamics, especially in the ground state. (iii) Accounts for quantum correlations (EC3) [6–8]. This unusual feature suggests a decoupling of protons from the chemical environment, in accordance with EC2, presumably due to hydrogen bonding. At the present stage of knowledge, we are not able to rationalize the physical or chemical origin of the decoupling. This should be regarded as an intrinsic feature of the KHCO_3 crystal that requires further investigations.

Finally, (iv) is a consequence of the rather large distances ($\approx 2.22 \text{ \AA}$) between nearest-neighbour protons. This is at variance with the proposal by Keen and Lovesey (KL) [16] and Lovesey [19] that quantum entanglement arises from the overlap integral S of the nuclear wave functions. However, this assumption is irrelevant; a straightforward estimate gives $S \sim 10^{-35}$ at 14 K [17]. Clearly, $S \equiv 0$ for all practical purposes.

3.1. The crystal of protons

Consider an ideal crystal composed of very large numbers N_a, N_b, N_c ($N = N_a N_b N_c$), of unit cells labelled j, k, l along the crystal axes $(a), (b), (c)$, respectively. For each unit cell there are two dimer entities (labelled A and B in Fig. 1) related through the (a, c) glide plane. These dimers are indexed as jkl and $j'kl$, respectively, with, not forgetting they are indistinguishable, $j = j'$. We start with the vibrational Hamiltonian for configuration **I** at $T = 0$

$$\mathcal{H}_0 = \mathcal{H}_H + \mathcal{H}_{\text{at}} + C_{\text{Hat}} \quad (1)$$

where \mathcal{H}_H and \mathcal{H}_{at} represent the sublattices of protons and heavy atoms (KCO_3), respectively, and C_{Hat} is a coupling term. In the harmonic approximation (ii) normal coordinates ξ_i are linear combinations of the normal coordinates x_r and X_s for \mathcal{H}_H and \mathcal{H}_{at} , respectively: $\xi_i = \sum_r \sum_s c_{rs} x_r X_s$. The gaussian wave functions $\Psi_{i,0}(\xi_i)$ are not factorable and cannot be antisymmetrized with respect to proton permutations. The fermionic nature is totally hidden, in conflict with (iii). Antisymmetrization is possible if, and only if, $C_{\text{Hat}} \equiv 0$ [6,8]. Hence, proton dynamics are totally decoupled from those of heavy atoms.

In order to explicit \mathcal{H}_H , we have to distinguish intra and inter-dimer coupling terms. The former splits the modes into u and g symmetry species [20]. The observed splitting for the three proton modes ($\Delta\nu/\nu \approx 5\%$) is a proof that the centre of symmetry holds at the time scale of proton dynamics. On the other hand, incoherent inelastic neutron scattering (INS) emphasizes that inter-dimer coupling terms are negligible [21]. Dynamics can be thus represented with virtually isolated centrosymmetric pairs of protons labelled $1jkl, 2jkl, 1j'kl$ and $2j'kl$, respectively. The harmonic Hamiltonian is then

$$\mathcal{H}_H = \sum_{j=j'=1}^{N_a} \sum_{k=1}^{N_b} \sum_{l=1}^{N_c} \sum_{\alpha} \{H_{jkl\alpha} + H_{j'kl\alpha}\}, \quad \alpha = x, y \text{ or } z; \quad (2)$$

$$H_{jkl\alpha} = \frac{1}{2m}(P_{1jkl\alpha}^2 + P_{2jkl\alpha}^2) + \frac{1}{2}m\omega_{0\alpha}^2[(\alpha_{1jkl} - \alpha_{0jkl})^2 + (\alpha_{2jkl} + \alpha_{0jkl})^2 + 2\lambda_\alpha(\alpha_{1jkl} - \alpha_{2jkl})^2];$$

$$j \leftrightarrow j': H_{jkl\alpha} \leftrightarrow H_{j'kl\alpha}.$$

$P_{1jkl\alpha}$ and $P_{2jkl\alpha}$ are kinetic momenta. Coordinates α_{1jkl} and α_{2jkl} are projections onto the α direction of proton positions, defined with respect to the projection of the centre of symmetry of the pair jkl . The frequency of uncoupled oscillators at equilibrium positions $\pm\alpha_{0jkl}$ is $\hbar\omega_{0\alpha}$. The coupling term shifts the equilibrium positions at $\pm\alpha'_{0jkl} = \pm\alpha_{0jkl}/(1 + 4\lambda_\alpha)$. The last line in (2) means that $H_{j'kl\alpha}$ is related to $H_{jkl\alpha}$ by substituting j' to j . For a dimer, normal coordinates (α_{ajkl} , α_{sjkl}) and conjugated momenta (P_{ajkl} , P_{sjkl})

$$\alpha_{sjkl} = \frac{1}{\sqrt{2}}(\alpha_{1jkl} - \alpha_{2jkl}),$$

$$P_{sjkl\alpha} = \frac{1}{\sqrt{2}}(P_{1jkl\alpha} - P_{2jkl\alpha}), \quad (3)$$

$$\alpha_{ajkl} = \frac{1}{\sqrt{2}}(\alpha_{1jkl} + \alpha_{2jkl}),$$

$$P_{ajkl\alpha} = \frac{1}{\sqrt{2}}(P_{1jkl\alpha} + P_{2jkl\alpha}),$$

split $H_{jkl\alpha}$ into uncoupled harmonic oscillators at frequencies $\hbar\omega_{\alpha\alpha} = \hbar\omega_{0\alpha}$ and $\hbar\omega_{s\alpha} = \hbar\omega_{0\alpha}\sqrt{1 + 4\lambda_\alpha}$, respectively, each with an effective mass $m_s = 1$ amu. The wave functions $\Psi_0^a(\alpha_{ajkl})$ and $\Psi_0^s(\alpha_{sjkl} - \sqrt{2}\alpha'_{0jkl})$ are nonlocal and nonfactorable. Protons are fully entangled into EPR-like states [22]. Then, we define the spatial wave functions either symmetrical or antisymmetrical with respect to permutation [6]

$$\Theta_{0jkl\pm} = \frac{1}{\sqrt{2}} \left[\prod_{\alpha} \Psi_0^a(\alpha_{ajkl}) \Psi_0^s(\alpha_{sjkl} - \sqrt{2}\alpha'_{0jkl}) \pm \prod_{\alpha} \Psi_0^s(\alpha_{ajkl}) \Psi_0^a(\alpha_{sjkl} + \sqrt{2}\alpha'_{0jkl}) \right], \quad (4)$$

and the antisymmetrized state vectors including spin states:

$$|0jkl+\rangle_H = |\Theta_{0jkl+}\rangle \otimes \frac{1}{\sqrt{2}}(|\uparrow_1\downarrow_2\rangle - |\downarrow_1\uparrow_2\rangle); \quad (5)$$

$$|0jkl-\rangle_H = |\Theta_{0jkl-}\rangle \otimes \frac{1}{\sqrt{3}}(|\uparrow_1\downarrow_2\rangle + \frac{1}{\sqrt{2}}|\uparrow_1\downarrow_2 + \downarrow_1\uparrow_2\rangle)$$

Eq. (3) defines ‘pseudoprotons’ (α_s , P_s) and (α_a , P_a) corresponding to symmetric or antisymmetric displacements of two half protons, respectively. The Pauli principle imposes (α_s , P_s) to be a singlet-like and (α_a , P_a) a triplet-like state, but, in contrast to magnetic systems, there is no spin–spin interaction, hence no splitting. Quantum entanglement is energy-free. It is dictated by the centre of symmetry and does not depend on the actual value of λ_α in (2).

Pseudoprotons become separable in excited vibrational states at $\sum_{\alpha} [(n_{\alpha a} + 1/2)\hbar\omega_{\alpha a} + (n_{\alpha s} + 1/2)\hbar\omega_{\alpha s}]$. The nonlocal

dynamics is preserved but the spin-symmetry is no longer required. This accords with a fundamental precept of quantum mechanics; energy transfer automatically destroys quantum entanglement.

Consider now the whole proton sublattice. According to (i), the ‘bosonization’ of dimers, analogous to Cooper pairs in superconductivity, or ^3He pairs in superfluidity, is not sufficient. Antisymmetrization must be realized for permutation of any two protons, wherever in the crystal, which automatically annihilates any wave across the sublattice. Hence, phonons are forbidden. The proton sublattice has no internal dynamics. It can be termed ‘superigid’. This macroscopic behaviour does not depend on any interaction between protons. It is dictated exclusively by the translational symmetry of the lattice.

Pseudoproton states can be thought of as superpositions of macroscopic single-particle states that are linear combinations of the state vectors (5):

$$|\overline{0\tau s}\rangle = \frac{1}{\sqrt{\bar{n}}} \left| \sum_{l=1}^{N_c} \sum_{k=1}^{N_b} \sum_{j=j'=1}^{N_a} [|0jkl\tau\rangle + s|0j'kl\tau\rangle] \right\rangle. \quad (6)$$

Here, $\tau = \pm$ for singlet and triplet states, $s = \pm 1$ for A or B symmetry species, respectively. The whole sublattice is a superposition of the degenerate and nonseparable states

$$|\bar{0}\rangle = \sqrt{\bar{n}} \sum_{\tau,s} |\overline{0\tau s}\rangle. \quad (7)$$

Local coordinates are totally hidden and permutation is now meaningless. These nonlocal states avoid any conflict with the symmetry postulate of quantum mechanics. They are not factorable and, according to (iv), there is no energy band structure.

Macroscopic entanglement is intrinsically decoherence-free. Upon irradiation by photons, neutrons, etc. transient disentanglement may single out some pseudoproton states as $\prod_{\alpha} |\bar{n}_{\alpha a}\rangle \otimes |\bar{n}_{\alpha s}\rangle$. However, after decaying to the ground state, re-entanglement occurs automatically at no energy cost, by virtue of indistinguishability. Massive decoherence is therefore cancelled out. Energy-free ‘re-entanglement’ on the time-scale of proton dynamics ($\sim 10^{-13}$ to 10^{-14} s) is the key mechanism keeping the sublattice at thermal equilibrium with the surroundings, despite the decoupling from heavy atoms and the lack of internal dynamics. Similarly, the sublattice of protons can adapt itself to structural changes with temperature and pressure. Note that even at room temperature, the thermal population of the lowest excited state for protons at $\approx 1000 \text{ cm}^{-1}$ is rather small ($\sim 10^{-2}$). The quantum entanglement of the ground state is prevailing, but the coherence length decreases as the temperature is increased. This, and possibly other mechanisms, accord with the broadening of the diffraction pattern visible at room temperature in Fig. 2.

For the deuterated analogue, KDCO_3 , Eqs. (4)–(7) are not necessary. The wave function $\prod_{\alpha} \Psi_0^a(\alpha_{ajkl}) \Psi_0^s(\alpha_{sjkl} - \sqrt{2}\alpha_{0jkl})$ is symmetrical with respect to permutation and spin correlation is not required. There is no entanglement. Dynamics are

represented as nonlocal pseudodeuterons according to (3) and phonons are allowed. Needless to say, the numbers of degrees of freedom are identical for the two systems. The main consequence of entanglement is to shrink the allowed Hilbert space from $\sim 12^n$ for bosons to $\sim 12n$ for fermions. (Note, there are 12 degrees of freedom per unit cells.)

3.2. Quantum interferences

Neutron scattering can be decomposed into distinct events. First, Bragg diffraction corresponding to nodes of the reciprocal lattice. Except at very particular nodes, decoherence upon momentum transfer takes place and the probability density is measured. Peak intensities are proportional to the Debye–Waller factor that is the Fourier transform of the self-correlation function [23].

Second, incoherent scattering, essentially by protons, gives an anisotropic continuum of intensity, with a Gaussian-like shape centered at $\mathbf{Q}=0$.

Third, quantum coherence is probed when components Q_x , Q_y , or Q_z correspond to nodes of the reciprocal sublattice of protons. Then, the coherent scattering cross section is dramatically increased by a factor of ≈ 45 , compared to that for Bragg diffraction.

The rods of diffuse scattering can be rationalized as follows. Protons in dimer planes are aligned along directions parallel to y (see dotted lines in Fig. 1) and quantum entanglement along this direction is equivalent to double lines of correlated scatterers with some similarity to well known double-slits experiments [6]. Neutron diffraction by such double-lines gives interference fringes [7]. Pursuing the same line of reasoning, macroscopic states in (x, y) planes form coherent grating-like structures in two dimensions that give sharp reflections for particular values of Q_x and Q_y . Finally, diffraction by the whole sublattice gives sharp peaks with dramatically enhanced intensities. All these events are effectively observed but a full discussion is beyond the frame of the present article. We shall limit the presentation to the ridges of diffuse scattering in Fig. 2.

In dimer planes, double-lines parallel to y (with an interline separation $2x'_0 \approx 0.6 \text{ \AA}$) form a grating-like structure that can be further decomposed into two subgratings corresponding to dimers A and B, respectively. The lattice periodicity of the subgratings is $D_x \approx a/\cos 42^\circ \approx 20.39 \text{ \AA}$. The differential cross-section for coherent scattering along Q_x , incoherent scattering along Q_z , and $Q_y=0$ is

$$\begin{aligned} \frac{d\sigma}{d\Omega} = & \sum_{\tau_i} \sum_{\tau_f} \sum_{k=1}^{N_b} \sum_{l=1}^{N_c} \left| \sum_{j=j'=1}^{N_a} \{b_{\text{H}jkl} [\exp iQ_x(jD_x - x'_0) \right. \\ & + \tau_f \tau_i \exp iQ_x(jD_x + x'_0)] + \tau_f \tau_i \exp i(Q_x D_x/2) \\ & \times b_{\text{H}'j'kl} [\exp iQ_x(j'D_x - x'_0) + \tau_f \tau_i \exp iQ_x(j'D_x + x'_0)] \} \Big|^2 \\ & \times \exp(-2W_z). \end{aligned} \quad (8)$$

Here, $\exp(-2W_z)$ is the Debye–Waller factor along z , and $b_{\text{H}jkl}$ is the scattering operator. The differential cross section diverges at $Q_x = \pm n_x \pi/x'_0 \approx \pm n_x 10 \text{ \AA}^{-1}$, for $\tau_i = \tau_f$ (in-phase scattering by double lines). Then, $Q_x D_x \approx \pm n_x 68\pi$ and $\tau_f \tau_i \exp i(Q_x D_x/2) = 1$. Neutrons are scattered in-phase by the two subgratings. The rods of intensity in Fig. 2 correspond to $n_x = 0, \pm 1$. (Rods anticipated at larger Q_x values are beyond the measured range.) Note that the phase matching condition, namely x'_0 be commensurable with D_x , is intrinsic to the crystal structure.

Alternatively, for anti-phase scattering by double-lines, $Q_x = \pm (n_x + 1/2)\pi/x'_0$ and $\tau_i \neq \tau_f$. Then, $\tau_f \tau_i \exp i(Q_x D_x/2) = -1$. Neutrons diffracted anti-phase by the two subgratings cancel out. There is no evidence indeed for such ridges at about ± 5 or $\pm 15 \text{ \AA}^{-1}$.

In conclusion, the ridges of diffuse scattering at low temperature are comprehensively interpreted as diffraction by the superigid sublattice of entangled protons.

4. Temperature effects: macroscopic resonant tunnelling states

At 300 K, the rods are virtually unaffected in position and direction, indicating that the essential features of the superigid lattice are preserved. This accords with a superposition of macroscopic states, say $|\mathbf{I}\rangle$ and $|\mathbf{II}\rangle$, corresponding to configurations **I** and **II**, respectively (Fig. 3). $|\mathbf{I}\rangle$ is identical to (7). Proton dynamics can be treated exactly in the same way for configuration **II** in order to construct single particle states $|\mathbf{II}\rangle$. The two configurations are not degenerate but the grating-like structures are identical and diffraction by the superlattice is unaffected by proton transfer.

According to quantum laws, the superposition of superigid states cannot account for proton transfer dynamics, because energy transfer yields disentanglement. Then, symmetric and

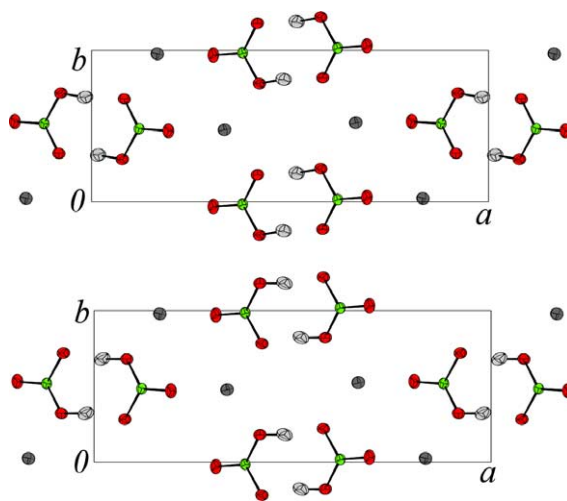


Fig. 3. Schematic view of entangled states $|\mathbf{I}\rangle$ (bottom) and $|\mathbf{II}\rangle$ (top) for coherent transfer of protons (for the interpretation of the reference to the colour in this legend, the reader is referred to the web version of this article).

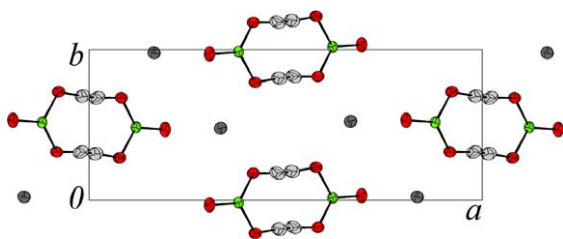


Fig. 4. Schematic view of the virtual disentangled state $2^{-1/2} [|\bar{\Pi}_a\rangle \otimes |\bar{\Pi}_s\rangle \pm |\bar{\Pi}_a\rangle \otimes |\bar{\Pi}_s\rangle]$. Each site is occupied by a half-proton (for the interpretation of the reference to the colour in this legend, the reader is referred to the web version of this article).

antisymmetric pseudoprotons become separable. The entangled states, each with $12N$ -fold degeneracy, split into four disentangled states, each with $6N$ -fold degeneracy:

$$|\bar{\Pi}_a\rangle \otimes |\bar{\Pi}_s\rangle \quad \text{at } 0; \quad (9)$$

$$2^{-1/2} [|\bar{\Pi}_a\rangle \otimes |\bar{\Pi}_s\rangle \pm |\bar{\Pi}_a\rangle \otimes |\bar{\Pi}_s\rangle] \quad \text{at } h\nu_{01};$$

$$|\bar{\Pi}_a\rangle \otimes |\bar{\Pi}_s\rangle \quad \text{at } 2h\nu_{01}.$$

The states $|\bar{\Pi}_a\rangle$ and $|\bar{\Pi}_a\rangle \otimes |\bar{\Pi}_s\rangle$ on the one hand, $|\bar{\Pi}_s\rangle$ and $|\bar{\Pi}_a\rangle \otimes |\bar{\Pi}_s\rangle$ on the other, are degenerate. Disentanglement/re-entanglement is energy-free. In the intermediate state, a pseudoproton is transferred across hydrogen bonds (Fig. 4). For the sake of simplicity, we suppose that the two intermediate states are degenerate, although a splitting would not change the overall scheme. The interconversion dynamics can be represented as a disentanglement/re-entanglement mechanism:

$$|\bar{\Pi}_a\rangle \otimes |\bar{\Pi}_s\rangle \pm |\bar{\Pi}_a\rangle \otimes |\bar{\Pi}_s\rangle \leftrightarrow |\bar{\Pi}_a\rangle \pm |\bar{\Pi}_s\rangle. \quad (10)$$

The energy level scheme for proton transfer dynamics is presented in Fig. 5. This is a two-stepwise process, each step corresponding to the transfer of a pseudoproton preserving the centre of symmetry. The ground state splitting observed with INS [21] can be therefore assigned to the intermediate state: $h\nu_{01} \approx 216 \text{ cm}^{-1}$.

The superposition of entangled states at thermal equilibrium

$$|\bar{\Psi}(T)\rangle = \bar{C}_I(T)|\bar{\Pi}_a\rangle + \bar{C}_{II}(T)|\bar{\Pi}_s\rangle, \quad (11)$$

with $\bar{C}_I^2(T) + \bar{C}_{II}^2(T) = 1$ gives the relative population of the less occupied site as

$$\bar{C}_{II}^2(T) = 2p_{01}^2(T)[1 + p_{01}^2(T)]^{-1}, \quad (12)$$

where $p_{01}(T) = \exp(-h\nu_{01}/kT)$. The estimate $\bar{C}_{II}^2 \approx 0.21$ at 300 K is in reasonable agreement with measurements (0.22). Alternatively, a superposition of the disentangled states would be

$$\begin{aligned} |\Psi(T)\rangle = & C_{00}(T)|\bar{\Pi}_a\rangle \otimes |\bar{\Pi}_s\rangle \\ & + 2^{-1/2} C_{01}(T)[|\bar{\Pi}_a\rangle \otimes |\bar{\Pi}_s\rangle + |\bar{\Pi}_a\rangle \otimes |\bar{\Pi}_s\rangle] \\ & + c_{11}(T)|\bar{\Pi}_a\rangle \otimes |\bar{\Pi}_s\rangle, \end{aligned} \quad (13)$$

with $C_{00}^2(T) + C_{01}^2(T) + C_{11}^2(T) = 1$. The population of the less

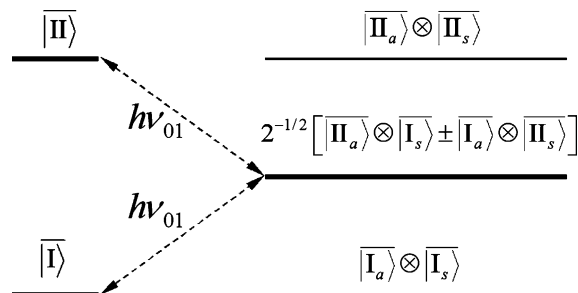


Fig. 5. Energy level scheme for entangled (left) and disentangled (right) configurations.

occupied site

$$\wp(T) = [p_{01}(T) + 2p_{01}^2(T)]P^{-1}(T), \quad (14)$$

with $P(T) = 1 + p_{01}(T) + p_{01}^2(T)$, would be ≈ 0.40 at 300 K, quite in variance with the observation. This emphasizes the impact of macroscopic entanglement onto the thermodynamics. The population degree of the intermediate state at $h\nu_{01}$ is clearly negligible and does not obey Boltzmann's law. This state is virtual; it does not exist if it is not 'measured'. In contrast, entangled states exist if they are not observed. Consequently, the double minimum potential function for single proton transfer is also virtual. (Presumably, it cannot be modelled with ab initio or whatsoever calculations.)

5. Conclusion

Neutron scattering experiments on KHCO_3 offer an opportunity to realize diffraction experiments by entangled double-lines of protons. At any temperature up to 300 K, the sublattice of protons is a superigid macroscopic quantum object. These experiments add crystalline solids to the list of substances with 'super' properties, along with liquids (superfluidity), vapour (Bose–Einstein condensate) and electrons (superconductivity).

The cornerstones of our theoretical framework are: (i) indistinguishability, (ii) time periodicity, (iii) the fermionic nature of protons, and (iv) degeneracy. The dynamics is rationalized with nonlocal pseudoprotons in macroscopic single-particle states. The superigid sublattice of pseudoprotons is perfectly decoupled from rest of the crystal and decoherence-free.

Up to room temperature, a number of pseudoprotons on the scale of Avogadro's constant is in a superposition of single-particle tunnelling states corresponding to distinct crystal configurations. There is no stochastic disordering and no transition from quantum to classical regime. Disentanglement gives rise to a virtual state for the transfer of pseudoprotons across a nonlocal double minimum potential. This view of proton transfer dynamics could be of importance to physics, chemistry and biology.

Acknowledgements

We are indebted to N. Leygue from LADIR, for preparing single crystals.

References

- [1] S. Benz, U. Haebleren, J. Tegenfeldt, Jump motion of deuterons along hydrogen bonds in KDCO_3 . A deuteron relaxation study, *J. Magn. Res.* 66 (1986) 125–134.
- [2] C. Odin, ^{13}C and ^{39}K high-resolution solid-state NMR study of the nonferroic phase transition of potassium hydrogen carbonate. Complementarity between NMR and incoherent neutron scattering, *J. Phys. Chem. B* 108 (2004) 7402–7411.
- [3] G. Eckold, H. Grimm, M. Stein-Arsic, Proton disorder and phase transition in KHCO_3 , *Physica B* 180–181 (1992) 336–338.
- [4] F. Fillaux, Calculation of infrared and raman band profiles of strong hydrogen bonds. OH stretching band and proton dynamics in crystalline potassium hydrogen carbonate, *Chem. Phys.* 74 (1983) 405–412.
- [5] F. Fillaux, Hydrogen bonding and quantum dynamics in the solid state, *Int. Rev. Phys. Chem.* 19 (2000) 553–564.
- [6] F. Fillaux, The Pauli principle and the vibrational dynamics of protons in solids: a new spin-related symmetry, *Physica D* 113 (1998) 172–183.
- [7] S. Ikeda, F. Fillaux, Incoherent–elastic–neutron scattering study of the vibrational dynamics and spin-related symmetry of protons in the KHCO_3 crystal, *Phys. Rev. B* 59 (1999) 4134–4145.
- [8] F. Fillaux, A. Cousson, D. Keen, Observation of the dynamical structure arising from spatially extended quantum entanglement and long-lived quantum coherence in the KHCO_3 crystal, *Phys. Rev. B* 67 (2003) (054301 and 189901(E)).
- [9] F. Fillaux, A. Cousson, M.J. Gutmann, Observation of quantum interference arising from a superposition of macroscopic tunnelling states for protons in the KHCO_3 crystal from 30 to 300 K, To be published
- [10] <http://www-llb.cea.fr>.
- [11] J.O. Thomas, R. Tellegren, I. Olovsson, Hydrogen-bond studies. LXXXIV. An X-ray diffraction study of the structures of KHCO_3 and KDCO_3 at 298, 219 and 95 K, *Acta Crystallogr. B* 30 (1974) 1155–1166.
- [12] J.O. Thomas, R. Tellegren, I. Olovsson, Hydrogen bond studies. XCII. Disorder in $(\text{HCO}_3)_2^{2-}$ and $(\text{DCO}_3)_2^{2-}$ dimers: a neutron diffraction study of KHCO_3 and KDCO_3 , *Acta Crystallogr. B* 30 (1974) 2540–2549.
- [13] V.M. Nield, D.A. Keen, *Diffuse Neutron Scattering from Crystalline Materials*, Oxford Series on Neutron Scattering in Condensed Matter, vol. 14, Clarendon Press, Oxford, 2001.
- [14] <http://www.isis.rl.ac.uk/crystallography>
- [15] By definition, the momentum transfer vector is $\mathbf{Q} = \mathbf{K}_\theta - \mathbf{K}_f$. \mathbf{K}_θ and \mathbf{K}_f are the incident and scattered wave vectors, respectively, with $\|\mathbf{K}_\theta\| = 2\pi/\lambda_\theta$ and $\|\mathbf{K}_f\| = 2\pi/\lambda_f$. Q_x , Q_y , Q_z are projections onto the three axes x , y , and z parallel to the ν OH, δ OH and γ OH modes, respectively (Fig. 1).
- [16] D.A. Keen, S.W. Lovesey, Quantum correlation between protons in potassium bicarbonate, *J. Phys.: Condens. Matter* 15 (2003) 4937–4946.
- [17] F. Fillaux, A. Cousson, Comment on quantum correlations between protons in potassium bicarbonate, *J. Phys.: Condens. Matter* 16 (2004) 1007–1010.
- [18] D.A. Keen, S.W. Lovesey, Reply to comment on quantum correlations between protons in potassium bicarbonate, *J. Phys.: Condens. Matter* 16 (2004) 5637–5638.
- [19] S.W. Lovesey, Quantum mechanical correlations between spatial and spin degrees of freedom in a material as revealed by neutron scattering, *Phys. Scripta* 71 (2) (2005) (cc14).
- [20] G. Lucazeau, A. Novak, Low temperature Raman spectra of KHCO_3 single crystal, *J. Raman Spectrosc.* 1 (1973) 573–586.
- [21] F. Fillaux, J. Tomkinson, J. Penfold, Proton dynamics in the hydrogen bond. The inelastic neutron scattering spectrum of potassium hydrogen carbonate at 5 K, *Chem. Phys.* 124 (3) (1988) 425–437.
- [22] A. Einstein, B. Podolsky, N. Rosen, Can quantum–mechanical description of physical reality be considered complete?, *Phys. Rev.* 47 (1935) 777–780.
- [23] S.W. Lovesey, *Nuclear Scattering, Theory of Neutron Scattered from Condensed Matter*, vol. 1, Clarendon Press, Oxford, 1984.